Lifting Line with Various Mollifications: Theory and Application to an Elliptical Wing

Denis-Gabriel Caprace*, Philippe Chatelain† and Grégoire Winckelmans‡.
Université catholique de Louvain, 1348 Louvain-la-Neuve, Belgium

Building on the well-known Prandtl Lifting Line (PLL), this work proposes an extended framework for mollified lifting lines, valid for multi-dimensional Gaussian smoothings. The smoothing length scale σ can be taken as constant or variable across the span. In this framework, a slender lifting device and its wake are represented by a mollified vortex tube and a mollified vortex sheet. While the resulting formulation is similar to the original one, it is shown that a sectional mean downwash must be used in the integro-differential equation from which the circulation distribution is obtained. Interestingly, it is also shown that this equation is unaffected by the presence of mollification in the streamwise direction. As an application, the case of the elliptical wing is revisited with several smoothing configurations. The results are consistent with the original singular lifting line, and the peculiarities of the circulation and downwash distributions are investigated. A uniform downwash is also recovered for a specific configuration. Finally, the constant and the variable σ regularizations are found to yield similar results. Overall, the proposed method provides accurate results which can be compared with those from numerical methods, such as the Actuator Line Model, Immersed Lifting Lines or other similar methods.

Nomenclature

α	=	geometrical angle of attack
a_0	=	slope of the airfoil lift coefficient
b	=	wing span
c	=	chord length
$\bar{c}$	=	mean aerodynamic chord
C_l	=	airfoil lift coefficient
δ	=	Dirac delta
D_i, D	=	induced and total drag force on the wing

*F.R.S.–FNRS Research Aspirant fellow, Institute of Mechanics, Materials and Civil Engineering (iMMC); denis-gabriel.caprace@uclouvain.be.
†Professor, iMMC; philippe.chatelain@uclouvain.be.
‡Full professor, iMMC; gregoire.winckelmans@uclouvain.be. Senior Member AIAA.

ε	=	local downwash angle
$\varepsilon_{\sigma,0}$	=	mollified downwash at the centerline
$\bar{\varepsilon}_{\sigma}$	=	mean regularized downwash
$\hat{\mathbf{e}}_x, \hat{\mathbf{e}}_y, \hat{\mathbf{e}}_z$	=	unit vector defining an orthonormal frame
$\mathbf{F}$	=	total force on the wing
Γ	=	circulation distribution
H	=	Heavyside step function
$\mathbf{K}\wedge$	=	3-D Biot-Savart kernel
$\mathbf{K}^{2D}\wedge$	=	2-D Biot-Savart kernel
L	=	lift force on the wing
ℓ	=	sectional lift of the airfoil
ρ	=	fluid density
S	=	surface of the wing
ζ	=	spanwise variable
$\mathbf{u}$	=	local velocity
u	=	local velocity component
$\mathbf{U}_0$	=	effective velocity
U_∞	=	norm of the upstream velocity
ξ_σ	=	regularization function
$\mathbf{x}$	=	spacial coordinate
$\boldsymbol{\omega}_\delta$	=	local singular vorticity
$\boldsymbol{\omega}_\sigma,\ \tilde{\boldsymbol{\omega}}_\sigma$	=	local regularized vorticity
ω	=	local vorticity component

Subscripts

0	=	evaluation at mid span or at the centerline
b	=	related to bound quantity
σ	=	mollified quantity
s	=	related to shed quantity

I. Introduction

The lifting line theory, originally formulated by Prandtl [1, 2] almost a century ago, is a very powerful tool to model the aerodynamics of a 3-D slender lifting device, in an unbounded domain. The simplicity of the formulation, together with the fact that it yields sensible results at a low computational cost, explains why it is still widely used in preliminary design of wings and for crude aerodynamics predictions. Still, the classical Prandtl Lifting Line (PLL) has its limitations: the represented lifting device must have a sufficiently high aspect ratio [**?**], $AR \geq 7 \ldots 8$. The latter condition ensures an error of less than 3% on the predicted effective lift slope of the device [9]. Moreover, it is constrained to straight geometries, where the aerodynamic center of every airfoil lies on a straight line (i.e. no sweep or dihedral). Small angles of attack and steady conditions are also assumed.

Researchers proposed variations and adaptations of the method in order to relax these strong assumptions and make it more general. Their thorough enumeration would be quite tedious; we can however mention efforts that worked toward a generalization of the theory, in order to make it compatible with curved, swept or arbitrary-shaped wings (among which [3, 4]), or to integrate unsteady aspects (see e.g. [5–7]). Several methods for solving the underlying numerical problem have also been proposed (e.g. [8–10])

More recently, the development of Computational Fluid Dynamics (CFD) has enabled the numerical resolution of 3-D complex flows past arbitrary geometries, with an ever increasing accuracy. However, the (very) high computational costs associated with large simulations sometimes prevent the use of body-resolved CFD, e.g. for the computation of the wake of complex machines such as full aircraft, rotorcraft, wind turbines, etc. For such applications, numerical methods derived from the PLL have been proposed in order to model the presence of the device in the flow.

One of the most popular modeling method is the Actuator Line Model (ALM), proposed by [11], which has been further developed and extensively used in the past decade (see e.g. [12, 13] for recent inputs and [14] for a review), for the Large Eddy Simulation (LES) of wind turbine wakes. The method consists in adding a source term in the Navier-Stokes equations to take into account the forces applied by the bodies (e.g. wings or blades) on the fluid. For numerical purposes, this force needs to be regularized on a grid using smoothing functions, often Gaussian. Generally, a good agreement with blade-resolved simulations is observed in terms of force distributions, despite some noticeable difficulties in the prediction of tip loads. Tip correction functions can be introduced in order to partially circumvent this issue [**?**].

While 3-D isotropic regularization functions with constant parameter were initially employed, it was proposed in [15, 16] to use a variable smoothing length scale in the spanwise direction, in order to improve the tip loads. Another variation of the ALMs was recently brought by the use of non-isotropic regularization functions in [17], stemming from the proposition that the shape of the regularization function should match the shape of the airfoil. In the latter work, distinct values for the smoothing length scale were used in the chord and thickness directions of an airfoil so as to maximize the likelihood between the potential flow around a resolved blade and the flow induced by the actuator line. Other smoothing functions were proposed through the Actuator Curve Embedding (ACE), where the regularization function is essentially 2-D [18] (i.e. $\sigma_y \ll \sigma_x, \sigma_z$), and with a significant improvement in the results at the tip.

Similar techniques have also been developed in flow solvers using the vorticity–velocity formulation of the Navier-

Stokes equations. We mention here the Immersed Lifting Line (ILL) approach, formulated in [19] using an Eulerian solver (the Vorticity Transport Model), and in [20–22] using a Lagrangian framework (the Vortex Particle-Mesh method). Both approaches were used to describe the physics of the wake of a Vertical Axis Wind Turbine.

In view of these numerical progresses, this paper comes back to the framework of the PLL in order to investigate the effect of smoothing on the theoretical circulation distribution and the induced velocities (downwash). The equations involved are written for the general case of 3-D regularization functions (also with variable spanwise smoothing), and are trivially extended to the case of anisotropic smoothing functions. The results obtained here are meant to shed light on the behavior of a mollified lifting line, and to provide high quality references for comparison with ALM, ILL and other similar methods. Indeed, in these methods, mollification has been extensively used as a necessary numerical ingredient, yet with a lack of theoretical background. Building on the mathematical framework introduced here, three key aspects of the mollification are here investigated in order to identify their respective influence: the shape of the regularization kernel, the definition of the downwash angle and the variation of the smoothing parameter along the span.

The paper is organized as follows: in Section II, we recall the classical PLL theory. Section III presents the framework leading to the mollified PLL with a uniform smoothing parameter. The method is developed for the specific cases of 3-D, 2-D and 1-D smoothing functions and applied to a wing with an elliptical planform. In Section IV, the case of a smoothing parameter scaling with the chord distribution of the wing is developed, and results for the elliptical wing are compared with those with uniform smoothing. Finally, conclusions are drawn in Section V.

II. Classical PLL

The classical lifting line theory uses the assumption of slender lifting devices, meaning that the span b (along the y direction) is significantly greater than any other dimension of the device (along x and z, see Fig. 1). Small angles of attack (AoA) are assumed everywhere. The device, represented by a straight line, is segmented in the spanwise direction. On each segment, we assume that the aerodynamics can be described using the 2-D (infinite span) relations, neglecting

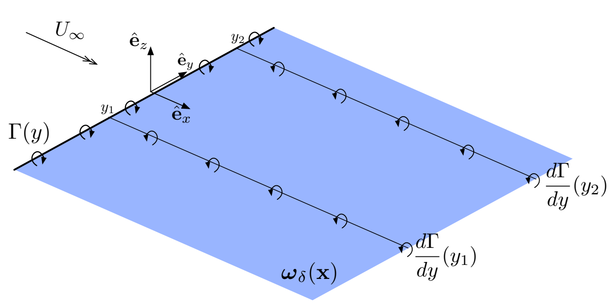

Fig. 1 Classical lifting line setup.

any transverse flow component. On the one hand, the Kutta-Joukowski theorem [23, 24] gives the sectional lift density

$$\ell(y) = \rho\, U_\infty\, \Gamma(y). \tag{1}$$

On the other hand, the definition of the sectional lift coefficient is

$$C_l(y) = \frac{\ell(y)}{\frac{1}{2}\rho\, U_\infty^2\, c(y)} = a_0\, \alpha_e(y)\,, \tag{2}$$

where the "effective angle of attack" is $\alpha_e(y) = \alpha - \varepsilon(y)$. In order to keep short expressions, the twist angle α_v is neglected in the following developments. However, the latter can easily be introduced as a modification in the effective angle of attack $\alpha_e(y) = \alpha + \alpha_v(y) - \varepsilon(y)$. The downwash angle $\varepsilon(y)$ is deduced from the Biot-Savart law which gives the velocity induced by the wake on the lifting line. In the original theory, the line is a singular vortex tube, and the wake is a singular vortex sheet. The vorticity field is thus also singular,

$$\boldsymbol{\omega}_\delta(\mathbf{x}) = \underbrace{\delta(x)\,\Gamma(y)\,\delta(z)}_{\omega_{\delta,b}}\ \hat{\mathbf{e}}_y + \underbrace{H(x)\,\left(-\frac{d\Gamma}{dy}(y)\right)\,\delta(z)}_{\omega_{\delta,s}}\ \hat{\mathbf{e}}_x, \tag{3}$$

where δ denotes the Dirac delta. The first term is the bound vorticity $\omega_{\delta,b}$ (i.e., the lifting line), and the second one is the shed vorticity $\omega_{\delta,s}$. The local velocity is

$$\mathbf{u}(\mathbf{x}) = U_\infty\, \hat{\mathbf{e}}_x + (\mathbf{K}(\mathbf{x})\wedge) * \boldsymbol{\omega}_\delta(\mathbf{x}), \tag{4}$$

with $(\mathbf{K}\wedge)$ the Biot-Savart kernel. Finally, the downwash angle, as measured on the lifting line, is

$$\varepsilon(y) = -\frac{\mathbf{u}(y)\cdot\hat{\mathbf{e}}_z}{U_\infty} = -\frac{1}{U_\infty}\frac{1}{2}\frac{1}{2\pi}\int_{-b/2}^{b/2}\frac{1}{(y-y')}\left(-\frac{d\Gamma}{dy'}\right)\,dy', \tag{5}$$

where the factor $\frac{1}{2}$ comes from the fact that the shed vortex lines go from $x = 0$ to $x = \infty$, and not from $x = -\infty$ to $x = \infty$. Combining Eqs. (1), (2) and the latter expression of the downwash angle leads to Prandtl's integro-differential equation,

$$\begin{aligned}\Gamma(y) &= \frac{1}{2}a_0\, c(y)\, U_\infty\, (\alpha - \varepsilon(y)) \\ &= \frac{1}{2}a_0\, c(y)\, U_\infty \left(\alpha - \frac{1}{U_\infty}\frac{1}{4\pi}\int_{-b/2}^{b/2}\frac{1}{(y-y')}\frac{d\Gamma}{dy'}\,dy'\right).\end{aligned} \tag{6}$$

As to the total lift and induced drag of the device, they are obtained as

$$\frac{L}{\rho} = U_\infty \int_{-b/2}^{b/2} \Gamma(y) dy \tag{7}$$

$$\frac{D_i}{\rho} = U_\infty \int_{-b/2}^{b/2} \varepsilon(y)\,\Gamma(y) dy, \tag{8}$$

again using the assumption of small angles.

III. Mollified PLL

We define regularization functions $\xi_\sigma(\mathbf{x})$, where σ is a smoothing length scale. In this work, Gaussian regularization functions are used. This allows to write $\xi_\sigma(\mathbf{x})$ as the product of 1-D functions $\xi_{\sigma_i}(x_i)$. Three types of regularization are here considered (as depicted in Figs. 2, 3 and 4):

- a 3-D isotropic Gaussian regularization:

$$\xi_\sigma(\mathbf{x}) = \xi_\sigma(x)\xi_\sigma(y)\xi_\sigma(z) = \frac{1}{\sqrt{\pi}^3\,\sigma^3}\left(e^{-\frac{x^2}{\sigma^2}}\right)\left(e^{-\frac{y^2}{\sigma^2}}\right)\left(e^{-\frac{z^2}{\sigma^2}}\right) = \frac{1}{\sqrt{\pi}^3\,\sigma^3} e^{-\frac{||\mathbf{x}||^2}{\sigma^2}}, \tag{9}$$

  Anisotropic cases (as in [17]) are also easily obtained as $\xi_{\sigma_x}(x)\xi_{\sigma_y}(y)\xi_{\sigma_z}(z)$, where different σ_i were used.

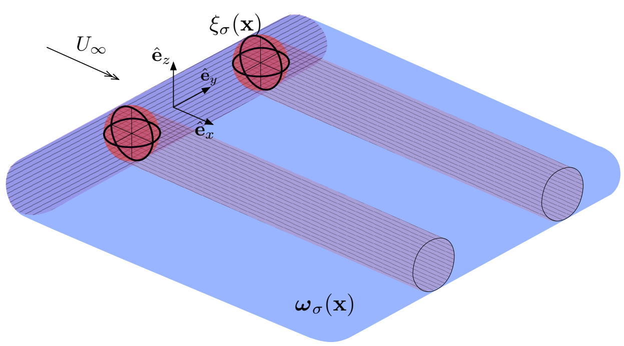

Fig. 2 3-D mollified lifting line setup (isotropic case)

- a 2-D (x-z slice) isotropic regularization:

$$\xi_\sigma(\mathbf{x}) = \xi_\sigma(x)\delta(y)\xi_\sigma(z) = \frac{1}{\pi\,\sigma^2}\left(e^{-\frac{x^2}{\sigma^2}}\right)\delta(y)\left(e^{-\frac{z^2}{\sigma^2}}\right), \tag{10}$$

  It corresponds to the 3-D regularization with $\sigma_y \to 0$ and $\sigma_x = \sigma_z = \sigma$, as in [18]. Anisotropic cases are also easily obtained using $\sigma_x \neq \sigma_z$.

- a 1-D (z, vertical) regularization:

$$\xi_\sigma(\mathbf{x}) = \delta(x)\delta(y)\xi_\sigma(z) = \frac{1}{\sqrt{\pi}\,\sigma}\delta(x)\,\delta(y)\left(e^{-\frac{z^2}{\sigma^2}}\right). \tag{11}$$

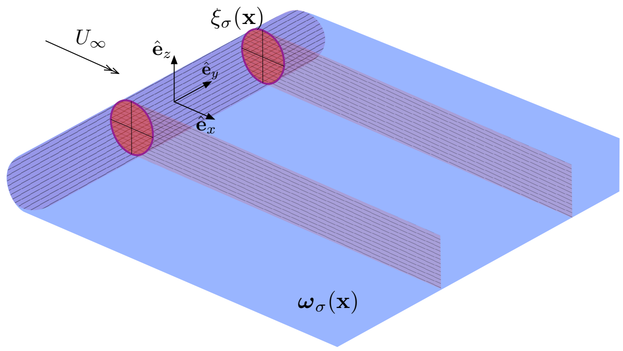

Fig. 3 2-D mollified lifting line setup (isotropic)

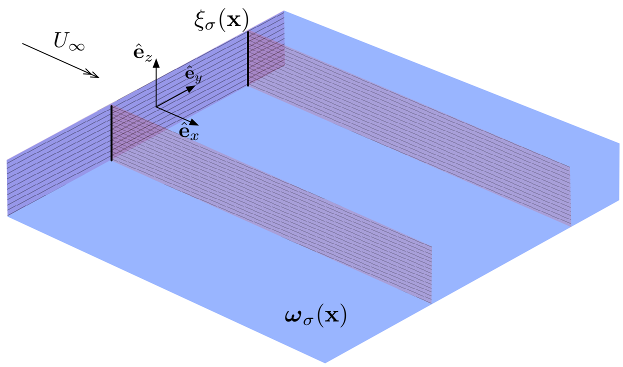

Fig. 4 1-D mollified lifting line setup

In all cases, we have that $\int_\Omega \xi_\sigma(\mathbf{x})\, d\Omega = 1$, with $\Omega = \mathbb{R}^3$. We first consider that σ is constant along the span. The case where σ varies in y is examined in Section IV. In the following development, we will obtain the expressions considering the case of a 3-D isotropic regularization.

The vorticity field, which was previously singular, becomes regular:

$$\begin{aligned}
\boldsymbol{\omega}_\sigma(\mathbf{x}) &= \xi_\sigma(\mathbf{x}) * \boldsymbol{\omega}_\delta(\mathbf{x}) \\
&= \underbrace{\int_{-b/2}^{b/2} \xi_\sigma(x, y-y', z)\, \Gamma(y')\, dy'}_{\omega_{\sigma,b}} \,\hat{\mathbf{e}}_y \\
&\quad + \underbrace{\int_{-b/2}^{b/2} \int_{-\infty}^{\infty} \xi_\sigma(x-x', y-y', z) \left(-H(x') \frac{d\Gamma}{dy}(y')\right) dx'\, dy'}_{\omega_{\sigma,s}} \,\hat{\mathbf{e}}_x \\
&= \xi_\sigma(x) \left(\int_{-b/2}^{b/2} \xi_\sigma(y-y')\, \Gamma(y')\, dy'\right) \xi_\sigma(z)\, \hat{\mathbf{e}}_y \\
&\quad + \underbrace{\left(\int_{-\infty}^{\infty} \xi_\sigma(x-x') H(x') dx'\right)}_{=\xi_\sigma(x) * H(x) = H_\sigma(x)} \left(\int_{-b/2}^{b/2} \xi_\sigma(y-y') \left(-\frac{d\Gamma}{dy}(y')\right) dy'\right) \xi_\sigma(z)\, \hat{\mathbf{e}}_x,
\end{aligned} \tag{12}$$

where we defined a mollified Heavyside function $H_\sigma(x) = \int_0^\infty \xi_\sigma(x - x')dx' = \frac{1}{2}[1 + \mathrm{erf}(x/\sigma)]$. It is worth noticing that the convolution of $\boldsymbol{\omega}_\delta$, which is solenoidal by construction, with a regularization kernel of prescribed σ, preserves its solenoidal property, $\nabla \cdot \omega_\sigma = 0$. The associated induced velocity field can be computed everywhere using the Biot-Savart (BS) law,

$$\begin{aligned}\mathbf{u}_\sigma(\mathbf{x}) &= U_\infty\,\hat{\mathbf{e}}_x + (\mathbf{K}(\mathbf{x})\wedge) * \boldsymbol{\omega}_\sigma(\mathbf{x}) \\ &= U_\infty\,\hat{\mathbf{e}}_x + (\mathbf{K}(\mathbf{x})\wedge) * (\omega_{\sigma,b}(\mathbf{x})\,\hat{\mathbf{e}}_y) + (\mathbf{K}(\mathbf{x})\wedge) * (\omega_{\sigma,s}(\mathbf{x})\,\hat{\mathbf{e}}_x) \\ &= U_\infty\,\hat{\mathbf{e}}_x + (\mathbf{K}_\sigma(\mathbf{x})\wedge) * (\omega_{\delta,b}(\mathbf{x})\,\hat{\mathbf{e}}_y) + (\mathbf{K}_\sigma(\mathbf{x})\wedge) * (\omega_{\delta,s}(\mathbf{x})\,\hat{\mathbf{e}}_x)\end{aligned} \tag{13}$$

where we used the 3-D BS kernel, $\mathbf{K}(\mathbf{x})\wedge = -(1/(4\pi\,||\mathbf{x}^3||))\,\mathbf{x}\wedge$. Notice that the associativity of the convolution product allows us to define the "mollified BS kernel", $\mathbf{K}_\sigma(\mathbf{x})\wedge = \xi_\sigma(\mathbf{x}) * \mathbf{K}(\mathbf{x})\wedge$. Taking advantage of the vector product of this kernel with the vorticity components of known orientation, we obtain the velocity components induced by the bound vorticity ($u_{\sigma,b,x}, u_{\sigma,b,z}$) and by the shed vorticity ($u_{\sigma,s,y}, u_{\sigma,s,z}$):

$$\mathbf{u}_\sigma(\mathbf{x}) = U_\infty\,\hat{\mathbf{e}}_x + \left(u_{\sigma,b,x}(\mathbf{x})\,\hat{\mathbf{e}}_x + u_{\sigma,b,z}(\mathbf{x})\,\hat{\mathbf{e}}_z\right) + \left(u_{\sigma,s,y}(\mathbf{x})\,\hat{\mathbf{e}}_y + u_{\sigma,s,z}(\mathbf{x})\,\hat{\mathbf{e}}_z\right). \tag{14}$$

For example, $u_{\sigma,b,x}$ is the x component ($_x$) of the velocity induced by the regularized ($_\sigma$) bound ($_b$) vorticity. The detailed expression of these velocity components can be found in the Appendix, together with their symmetry properties which will be invoked in the following developments.

In the singular case, the Kutta-Joukowski theorem (Eq. (1)) was used. Because of the mollification however, it can no longer be used to relate the circulation and the sectional lift. As mentioned in [4], we will rather rely on the general 3-D vortex lifting law demonstrated in [25, 26],

$$\frac{\mathbf{F}}{\rho} = \int_\Omega \mathbf{u}_\sigma(\mathbf{x}) \wedge \omega_\sigma(\mathbf{x})\,d\mathbf{x}. \tag{15}$$

In the particular case of a singular vortex line, it becomes

$$\frac{\mathbf{F}}{\rho} = \int_{-b/2}^{b/2} \mathbf{u}_0(y) \wedge (\Gamma(y)\hat{\mathbf{e}}_y)\,dy,$$

where $\mathbf{u}_0$ is an effective velocity: the velocity as seen by the lifting line. Under the small angle assumption, $\mathbf{u}_0(y) = U_\infty\hat{\mathbf{e}}_x - \varepsilon(y)U_\infty\hat{\mathbf{e}}_z$ and we recover the classical results for the lift and induced drag forces.

Equation (15) can be reworked using the regularized velocity components, Eq. (14), and the vorticity components, Eq. (12) in order to obtain a simpler expression. Taking advantage of the known symmetries of these components (found in the Appendix) and their product, only a few terms remain after the integration of the cross product over Ω,

$$
\begin{aligned}
\frac{\mathbf{F}}{\rho} = & \left(\int_\Omega U_\infty \, \omega_{\sigma,b}(\mathbf{x}) \, d\mathbf{x} \right) \hat{\mathbf{e}}_z - \left(\int_\Omega u_{\sigma,s,z}(\mathbf{x}) \, \omega_{\sigma,b}(\mathbf{x}) \, d\mathbf{x} \right) \hat{\mathbf{e}}_x \\
& + \left(\int_\Omega u_{\sigma,b,z}(\mathbf{x}) \, \omega_{\sigma,s}(\mathbf{x}) \, d\mathbf{x} \right) \hat{\mathbf{e}}_y + \left(\int_\Omega u_{\sigma,s,z}(\mathbf{x}) \, \omega_{\sigma,s}(\mathbf{x}) \, d\mathbf{x} \right) \hat{\mathbf{e}}_y .
\end{aligned}
\tag{16}
$$

The latter expression results from the fact that the integral over the domain of an odd function is zero. We finally obtain the expressions for the lift and induced drag forces using projections of $\frac{\mathbf{F}}{\rho}$ along z and x,

$$
\frac{L}{\rho} = U_\infty \int_\Omega \xi_\sigma(x) \left(\int_{-b/2}^{b/2} \xi_\sigma(y - y') \, \Gamma(y') \, dy' \right) \xi_\sigma(z) \, d\mathbf{x} = U_\infty \int_{-b/2}^{b/2} \Gamma(y) dy \tag{17}
$$

$$
\frac{D_i}{\rho} = - \int_\Omega u_{\sigma,s,z}(\mathbf{x}) \, \omega_{\sigma,b}(\mathbf{x}) \, d\mathbf{x} = U_\infty \int_{-b/2}^{b/2} \bar{\varepsilon}_\sigma(y) \, \Gamma(y) dy, \tag{18}
$$

where $\bar{\varepsilon}_\sigma(y)$ is an effective "sectional mean downwash" (see below). As expected, the expression for the lift force is identical to that of the singular case.

In order to derive the right-hand side of the mollified Prandtl integro-differential equation, we will obtain another expression for the lift by introducing a regularization of the lift coefficient. In the general case of a 3-D mollification, the support of $\mathbf{u}_\sigma$ and ω_σ is $\mathbb{R}^3$ and we will obtain that the total force is the sum of every infinitesimal contribution from any point in that space. In other words, we need to define a local lift coefficient for all $\mathbf{x}$; to this end, we define a "regularized chord". Considering that the chord distribution can be expressed as a singular distribution in 3-D, $c_\delta(\mathbf{x}) = \delta(x)\delta(y)c(y)$, we define $c_\sigma(\mathbf{x}) = \xi_\sigma(\mathbf{x}) * c_\delta(\mathbf{x}) = \xi_\sigma(x) \left(\int_{-b/2}^{b/2} \xi_\sigma(y - y') \, c(y') \, dy' \right) \xi_\sigma(z)$, which satisfies $\int_\Omega c_\sigma(\mathbf{x}) \, d\mathbf{x} = \int_{-b/2}^{b/2} c(y) \, dy = S$, with S being the wing surface. In the case of the 2-D or the 1-D mollification defined above, where there is no mollification in the spanwise direction, $c_\sigma(\mathbf{x})$ can readily be replaced by $c(y)$ times the 2-D (or 1-D) mollification kernel.

It is now possible to express the lift as the integral over Ω of the mollified lift coefficient. We obtain

$$
L = \frac{1}{2} \rho U_\infty^2 \int_\Omega c_\sigma(\mathbf{x}) \, \left(a_0 \big(\alpha - \varepsilon_\sigma(\mathbf{x}) \big) \right) d\mathbf{x}, \tag{19}
$$

with the regularized downwash angle $\varepsilon_\sigma(\mathbf{x}) = -\frac{\mathbf{u}_\sigma(\mathbf{x}) \cdot \hat{\mathbf{e}}_z}{U_\infty}$. By equating this expression and Eq. (17), we obtain

$$
\begin{aligned}
\int_{-b/2}^{b/2} \Gamma(y)\, dy &= \frac{1}{2} a_0\, U_\infty \int_\Omega \Big(\xi_\sigma(\mathbf{x}) * c_\delta(\mathbf{x})\Big) \Big(\alpha - \varepsilon_\sigma(\mathbf{x})\Big) d\mathbf{x} \\
&= \frac{1}{2} a_0\, U_\infty \int_\Omega c_\delta(\mathbf{x}) \Big((\xi_\sigma(\mathbf{x}) * \alpha) - (\xi_\sigma(\mathbf{x}) * \varepsilon_\sigma(\mathbf{x})) \Big) d\mathbf{x} \\
&= \frac{1}{2} a_0\, U_\infty \int_{-b/2}^{b/2} c(y) \Big(\alpha - \left[\xi_\sigma(\mathbf{x}) * \varepsilon_\sigma(\mathbf{x})\right]_{x=z=0}\Big) dy,
\end{aligned}
\tag{20}
$$

where the last equality is obtained using the above definition of $c_\delta(\mathbf{x})$. We used the associative property of the convolution, which is here a keystone of all developments.

Importantly, the last result leads us to define the *sectional mean downwash angle* (simply referred to as mean downwash hereafter),

$$
\bar{\varepsilon}_\sigma(y) = -\frac{1}{U_\infty} \Big(\left[\xi_\sigma(\mathbf{x}) * \mathbf{u}_\sigma(\mathbf{x})\right]_{x=z=0} \Big) \cdot \hat{\mathbf{e}}_z . \tag{21}
$$

Invoking symmetry properties again, the only non-zero contribution to the convolution comes from the velocity induced by the vorticity shed in the wake (through $u_{\sigma,s,z}$, cfr. Appendix),

$$
\bar{\varepsilon}_\sigma(y) = -\frac{1}{U_\infty} \int_\Omega \xi_\sigma(x', y - y', z')\, u_{\sigma,s,z}(\mathbf{x}') d\mathbf{x}'. \tag{22}
$$

A natural way to satisfy Eq. (20) is to write

$$
\Gamma(y) = \frac{1}{2} a_0\, U_\infty\, c(y)\, (\alpha - \bar{\varepsilon}_\sigma(y)), \tag{23}
$$

which can be viewed as the equivalent Prandtl integro-differential equation for the regularized lifting line, and which indeed uses the mean downwash angle as the effective one. We notice the strong similarity between the equation just formulated and Eq. (6) for the singular case.

It is also worth noticing that Eq. (17) could have been decomposed so as to identify a sectional lift, as performed in the singular case,

$$
\begin{aligned}
\frac{\ell_\sigma(y)}{\rho} &= U_\infty \int_{-\infty}^{\infty} \int_{-\infty}^{\infty} \int_{-b/2}^{b/2} \xi_\sigma(x', y - y', z')\, \Gamma(y')\, dy'\, dx'\, dz' \\
&= U_\infty \int_{-b/2}^{b/2} \xi_\sigma(y - y')\, \Gamma(y')\, dy' = U_\infty\, \Gamma_\sigma(y).
\end{aligned}
\tag{24}
$$

A mollified circulation distribution Γ_σ appears, which is the circulation that would be measured in the domain by applying the definition $\Gamma = \oint \mathbf{u} \cdot d\mathbf{l}$. This quantity can be related to the mollified lift coefficient, integrated over a section, through

$$\Gamma_\sigma(y) = \frac{1}{2} U_\infty \int_{-\infty}^{\infty}\int_{-\infty}^{\infty} \Big(\xi_\sigma(\mathbf{x}) * c(\mathbf{x})\Big)\, a_0\Big(\alpha - \varepsilon_\sigma(y)\Big) dx\, dz, \tag{25}$$

where the convolution does not commute with the multiplication, due to the absence of the integral in y. We stress that, although $\frac{L}{\rho} = \int_{-\infty}^{\infty} \Gamma(y)\, dy = \int_{-\infty}^{\infty} \Gamma_\sigma(y)\, dy$, it is not true that $\Gamma_\sigma(y) = \Gamma(y)$ if the mollification kernel also acts in y. In that case, the circulation distribution $\Gamma(y)$ is not readily accessible from the integration of ω_σ on a section.

The definition of the mean downwash (Eq. (21)) recalls the *integral velocity sampling* proposed in [12] for the computation of the effective angle of attack in an ALM. Indeed, we here demonstrated the necessity of using a mean downwash to maintain the consistency of the approach. The mean downwash is obtained through an additional convolution of the regularized velocity with the regularization function ξ_σ. We recall that the mathematical reasoning developed here holds in a fully 3-D framework.

This being said, it is worth mentioning that another option for defining the effective downwash angle to be used in Eq. (23) would be

$$\varepsilon_{\sigma,0}(y) = -\frac{1}{U_\infty}\Big[\mathbf{u}_\sigma(\mathbf{x}) \cdot \hat{\mathbf{e}}_z\Big]_{x=z=0}, \tag{26}$$

i.e. the local downwash angle resulting from the evaluation of the regularized downwash at the "center" of the line. Although it is formally not consistent with the regularized approach developed above, many implementations of the ALM use the latter definition for the effective downwash angle. In what follows, we will therefore also consider the solution of Eq. (23) with that centerline downwash angle, and compare the results to those obtained when using the mean downwash angle.

In the remainder of this section, Eq. (23) is particularized to the cases of a 3-D Gaussian regularization in Section III.A, a 2-D Gaussian regularization in Section III.B, and a 1-D Gaussian regularization in Section III.C.

A. 3-D Gaussian Regularization

1. Mean and Centerline Downwash Expressions

We recall the 3-D Gaussian isotropic regularization kernel (Eq. (9)), spanning over the three dimensions,

$$\xi_\sigma(\mathbf{x}) = \xi_\sigma(x)\xi_\sigma(y)\xi_\sigma(z) = \frac{1}{\sqrt{\pi}^3\,\sigma^3} e^{-\frac{\|\mathbf{x}\|^2}{\sigma^2}}.$$

The vertical velocity induced by the wake, required for the evaluation of the downwash angle, can be obtained by computing the integral given in the Appendix. We use the mollified Biot-Savart kernel convoluted with the singular voriticty field $\boldsymbol{\omega}_{\delta,s}$,

$$u_{\sigma,s,z}(\mathbf{x}) = (\mathbf{K}_\sigma(\mathbf{x}) \cdot \hat{\mathbf{e}}_y) * \left(H(x) \left(-\frac{d\Gamma}{dy}(y) \right) \delta(z) \right) \tag{27}$$

$$\begin{aligned} &= -\frac{1}{4\pi} \int_{-b/2}^{b/2} \frac{1}{\sigma\rho} \Bigg[\left(1 - e^{-\rho^2}\right) \\ &\quad - \left(\frac{x/\sigma}{\sqrt{\rho^2 + x^2/\sigma^2}} \operatorname{erf}\left(\sqrt{\rho^2 + \frac{x^2}{\sigma^2}} \right) - e^{-\rho^2} \operatorname{erf}\left(\frac{x}{\sigma}\right) \right) \\ &\quad - \frac{1}{\sqrt{\pi}} \frac{x}{\sigma} \left(e^{-x^2/\sigma^2} - e^{-\rho^2 - x^2/\sigma^2} \right) \Bigg] \frac{d\Gamma}{dy}(y') dy', \end{aligned} \tag{28}$$

where $\rho^2 = \frac{(y-y')^2+z^2}{\sigma^2}$. More details about this can be found in Appendix B of [27].

On the one hand, the centerline downwash angle (Eq. (26)) corresponds to the evaluation of this expression at $x = z = 0$,

$$\varepsilon_{\sigma,0}(y) = -\frac{1}{U_\infty} \frac{1}{4\pi} \int_{-b/2}^{b/2} \frac{\left(1 - e^{-\frac{(y-y')^2}{\sigma^2}}\right)}{(y - y')} \frac{d\Gamma}{dy}(y') dy'. \tag{29}$$

On the other hand, the mean downwash angle (Eq. (21)) requires the evaluation $\xi_\sigma(\mathbf{x}) * \mathbf{u}_\sigma(\mathbf{x}) = \xi_\sigma(\mathbf{x}) * \xi_\sigma(\mathbf{x}) * \mathbf{u}(\mathbf{x})$. Using the important property that the convolution of a Gaussian function of smoothing parameter σ with itself leads to a Gaussian function of smoothing parameter equal to $\sqrt{2}\sigma$, the mean downwash finally corresponds to

$$\bar{\varepsilon}_\sigma(y) = \frac{1}{U_\infty} \frac{1}{4\pi} \int_{-b/2}^{b/2} \frac{\left(1 - e^{-\frac{(y-y')^2}{2\sigma^2}}\right)}{(y - y')} \frac{d\Gamma}{dy}(y') dy'. \tag{30}$$

Note Interestingly, the exact same result can be obtained from a mollification without regularization in the streamwise direction. Let's define a Gaussian regularization kernel spanning over y and z,

$$\xi_\sigma^{YZ}(\mathbf{x}) = \delta(x) \left(\frac{1}{\pi\sigma^2} e^{-\frac{(y^2+z^2)}{\sigma^2}} \right). \tag{31}$$

In this particular case, the velocity induced on the support of the attached vorticity (i.e. $x = 0$) is

$$\begin{aligned} u_{\sigma,s,z}^{YZ}(y,z) &= \frac{1}{2} \left((\mathbf{K}_\sigma^{2D}(y,z)) * \left(-\frac{d\Gamma}{dy}(y)\, \delta(z) \right) \right) \cdot \hat{\mathbf{e}}_z \\ &= -\frac{1}{2} \frac{1}{2\pi} \int_{-b/2}^{b/2} \frac{\left(1 - e^{-\frac{\left((y-y')^2+z^2\right)}{\sigma^2}}\right)}{(y-y')^2 + z^2} (y - y') \frac{d\Gamma}{dy}(y') dy', \end{aligned} \tag{32}$$

where, in this specific case, we used a 2-D convolution and the (y-z) mollified Biot-Savart kernel. The expressions for the downwash angles are then

$$\varepsilon_{\sigma,0}^{YZ}(y) = \frac{1}{U_\infty}\frac{1}{4\pi}\int_{-b/2}^{b/2}\frac{\left(1 - e^{-\frac{(y-y')^2}{\sigma^2}}\right)}{(y-y')}\frac{d\Gamma}{dy}(y')dy', \tag{33}$$

and

$$\bar{\varepsilon}_{\sigma}^{YZ}(y) = \frac{1}{U_\infty}\frac{1}{4\pi}\int_{-b/2}^{b/2}\frac{\left(1 - e^{-\frac{(y-y')^2}{2\sigma^2}}\right)}{(y-y')}\frac{d\Gamma}{dy}(y')dy'. \tag{34}$$

These are exactly the same expressions as those obtained with the 3-D regularization. This conclusion suggests that the mollification in the streamwise direction has no influence on the formulation of the problem.

2. *Application to an Elliptical Wing*

The constant parameter mollified PLL method is applied to the case of a wing of aspect ratio $AR = 20$ with an elliptical chord distribution, and compared to the classical PLL method for which the solution is the elliptical circulation distribution. We note that this very high aspect ratio is typical of wind turbine blades; todays commercial aircraft wings generally have more moderate aspect ratios ($AR = 7...10$). Nevertheless, the selection of a specific aspect ratio does not really matter when discussing the influence of the mollification, at least for $AR \geq 7...8$. The particular case of the elliptical circulation distribution was elected for its significance to the classical PLL, which yield the minimum induced drag and a constant downwash distribution. All results presented below were obtained by numerically solving Eq. (23), using the downwash angle expressions of Eqs. (29) and (30).

We first study the influence of the parameter σ/b on the circulation distribution and on the mean downwash angle. This ratio is the core parameter governing the level of influence of the mollification on the results. The aspect ratio, on the other hand, contributes to a much lesser extent in the study of the mollification, and will therefore not be varied here. The distributions are made non-dimensional using the circulation at mid-span Γ_0 and the uniform downwash angle ε_0 obtained with the classical PLL. We recall that $L = \rho\, U_\infty\, \Gamma_0\, b_0$. For the elliptical wing with $\Gamma_{\text{ref}}(y)/\Gamma_0 = \sqrt{1 - \left(\frac{y}{b/2}\right)^2}$, the classical PLL gives $b_0 = \frac{\pi}{4}b$ and and $C_{D_i} = \frac{1}{\pi\, AR}C_L^2$. Therefore,

$$C_{L,\text{ref}} = \frac{\pi}{2}\frac{\Gamma_0}{U_\infty}\frac{AR}{b}$$

and

$$C_{D_i,\text{ref}} = \frac{\pi}{4}\frac{\Gamma_0^2}{U_\infty^2}\frac{AR}{b^2}.$$

Figure 5 shows the circulation distribution computed with the mollified PLL. It deviates from the ellipse, Γ_{ref}, with

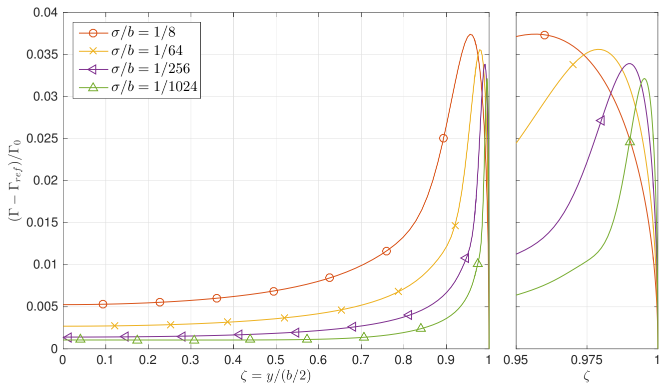

Fig. 5 Difference between the circulation distribution of the mollified PLL and the elliptical distribution, for a 3-D regularization kernel with mean downwash evaluation and constant σ along the span.

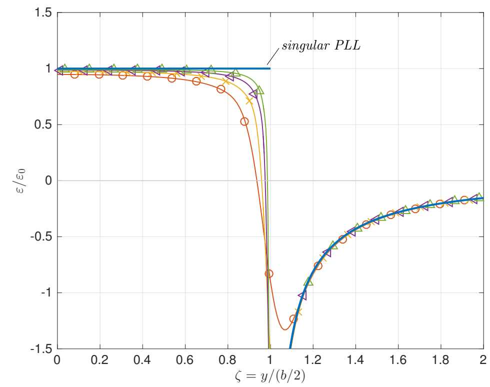

Fig. 6 Downwash angle on the mollified PLL for a 3-D regularization kernel, with mean downwash evaluation and constant σ along the span.

an overall increase in circulation over the wing. The maximum difference is observed in the tip region and decreases for decreasing values of σ; it never exceeds 4 percent of the circulation at mid-span for the "large" σ case, though. Of course, the circulation at the tip is zero for all regularizations in order to enforce the zero lift condition. It can be seen that the regularized method is consistent with the classical PLL results when $\sigma \to 0$, with a behavior close to linear as far as the 2-norm is concerned (see Table 1). Yet, the maximum value of $(\Gamma - \Gamma_{\mathrm{ref}})$ decreases at a reduced rate with σ/b.

As a consequence of the increased circulation over the wing, the lift coefficient C_L is slightly higher than the reference one. In other words, for a given lift coefficient, the mollified wing would fly at a slightly lower angle of attack than the singular one, and with less induced drag.

This observation is explained by the smaller downwash angle obtained on the mollified PLL (see Fig. 6). While the reference case has a constant downwash angle along the wing, and a singular behavior at the tip, the smoothing introduced here results in the continuity of the downwash angle and of its derivative. Consequently, the downwash angle is lower than the reference in the tip region, therefore inducing a lower contribution of the tip region to the induced drag. In the tip region, a portion of the wing (the size of which decreases with σ) even benefits from an upwash velocity. There, the lift vector is tilted forward and induces thrust.

σ/b	$\frac{C_L}{C_{L,ref}}$	$\frac{C_{D_i}}{C_{D_i,ref}}$	$\lVert\Gamma - \Gamma_{\mathrm{ref}}\rVert_2$	$\lVert\Gamma - \Gamma_{\mathrm{ref}}\rVert_\infty$
1/32	1.014	0.871	0.183	0.037
1/64	1.008	0.925	0.082	0.036
1/128	1.005	0.957	0.036	0.034
1/256	1.003	0.976	0.016	0.032

Table 1 Lift and drag coefficients on the mollified PLL for a 3-D regularization kernel, with constant σ along the span.

B. 2-D (Slice) Gaussian Regularization

1. Mean and Centerline Downwash Expressions

We recall the 2-D Gaussian isotropic regularization kernel (Eq. (10)), spanning over the streamwise and vertical directions,

$$\xi_\sigma(\mathbf{x}) = \xi_\sigma(x)\delta(y)\xi_\sigma(z) = \frac{1}{\pi\,\sigma^2}\left(e^{-\frac{(x^2+z^2)}{\sigma^2}}\right)\delta(y).$$

There is thus no regularization in the spanwise direction. Incidentally, this is what the Actuator Curve Embedding (ACE) [18] aims at doing: a cancelation of the filtering effect in y on the aerodynamic distributions. In the ACE however, the regularization kernel cannot be infinitely thin. The force acting on each segment is distributed in a very narrow region in y, so that there is always a small overlap of the kernel between two adjacent segments (meaning that the size of the smoothing in y is larger than the distance between nearby collocation points). In our 2-D regularization, the kernel is effectively infinitely thin in y, and no effect of explicit filtering will be observed in that direction. In particular, we have $\Gamma_\sigma(y) = \Gamma(y)$, meaning that the circulation measured on a cross-section of the lifting line is equal to the one of interest.

The vertical velocity induced by the vorticity in the wake is computed using the 3-D Biot-Savart law on the mollified vorticity $\boldsymbol{\omega}_{\sigma,s}$,

$$\begin{aligned} u_{\sigma,s,z}(\mathbf{x}) &= \left((\mathbf{K}(y,z)) * \left(H_\sigma(x)\left(-\frac{d\Gamma}{dy}(y)\right)\xi_\sigma(z)\right)\right)\cdot\hat{\mathbf{e}}_z \\ &= \frac{1}{4\pi}\int_{-\infty}^{\infty}\int_{-b/2}^{b/2}\int_{-\infty}^{\infty}\frac{(y-y')}{||\mathbf{x}-\mathbf{x}'||^3}\,\frac{(1+\mathrm{erf}(\frac{x'}{\sigma}))}{2}\left(-\frac{d\Gamma}{dy}(y')\right)\frac{e^{\frac{-z'^2}{\sigma^2}}}{\sqrt{\pi}\,\sigma}dx'\,dy'\,dz'. \end{aligned} \tag{35}$$

Evaluating the velocity at the centerline leads to the expression for the centerline downwash angle,

$$\begin{aligned} \varepsilon_{\sigma,0}(y) &= \frac{1}{U_\infty}\frac{1}{4\pi}\int_{-b/2}^{b/2}\left(\int_{-\infty}^{\infty}\left[\int_{-\infty}^{\infty}\frac{H_\sigma(x')}{(x'^2+(y-y')^2+z'^2)^{\frac{3}{2}}}dx'\right]\frac{e^{\frac{-z'^2}{\sigma^2}}}{\sqrt{\pi}}\frac{dz'}{\sigma}\right)(y-y')\frac{d\Gamma}{dy}(y')\,dy' \\ &= \frac{1}{U_\infty}\frac{1}{4\pi}\int_{-b/2}^{b/2}\left(\int_{-\infty}^{\infty}\frac{1}{\sqrt{\pi}}\frac{e^{-\frac{z'^2}{\sigma^2}}}{((y-y')^2+z'^2)}\frac{dz'}{\sigma}\right)(y-y')\frac{d\Gamma}{dy}(y')\,dy' \\ &= \frac{1}{U_\infty}\frac{1}{4\pi}\int_{-b/2}^{b/2}g\left(\frac{|y-y'|}{\sigma}\right)\frac{1}{(y-y')}\frac{d\Gamma}{dy}(y')\,dy', \end{aligned}$$

where we defined the function $g(s) = \frac{s^2}{\sqrt{\pi}}\int_{-\infty}^{\infty}\frac{e^{-t^2}}{(t^2+s^2)}\,dt$ which has a primitive (see Faddeeva function in [28, Eqs. (7.2.3) and (7.7.2)]): $g(s) = \sqrt{\pi}\,s\,e^{s^2}\,\mathrm{erfc}(s)$. This function is normalized such that $g(0) = 0$ and $\lim_{s\to\infty} g(s) = 1$. Therefore, we finally obtain

$$\varepsilon_{\sigma,0}(y) = \frac{1}{U_\infty}\frac{1}{4\pi}\int_{-b/2}^{b/2}\left[\sqrt{\pi}\frac{|y-y'|}{\sigma}\,\mathrm{erfc}\left(\frac{|y-y'|}{\sigma}\right)e^{\frac{|y-y'|^2}{\sigma^2}}\right]\frac{1}{(y-y')}\frac{d\Gamma}{dy}(y')\,dy'. \tag{36}$$

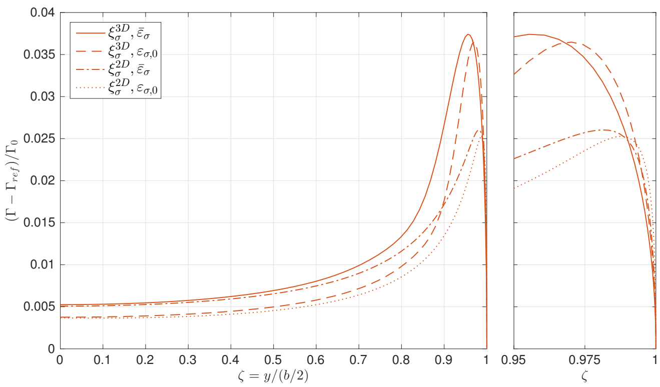

Fig. 7 Difference between the circulation distribution of the mollified PLL and the elliptical distribution, obtained with the 3-D and the 2-D (or 1-D) mollifications, and with constant σ along the span ($\sigma/b = 1/32$).

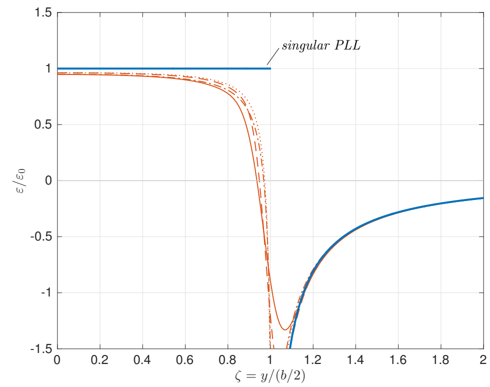

Fig. 8 Mean and centerline evaluation of the downwash angle for the 3-D and the 2-D (or 1-D) mollified PLL with constant σ along the span ($\sigma/b = 1/32$).

For the mean downwash angle, we introduce the additional convolution,

$$\begin{aligned}\bar{\varepsilon}_\sigma(y) &= \frac{1}{U_\infty}\frac{1}{4\pi}\int_{-b/2}^{b/2}\left(\iint_{-\infty}^{\infty}\left[\iint_{-\infty}^{\infty}\frac{H_\sigma(x')\,\frac{e^{\frac{-x^2}{\sigma^2}}}{\sqrt{\pi}}}{||\mathbf{x}-\mathbf{x}'||^3}\,dx\,dx'\right]\frac{e^{-\frac{z^2+z'^2}{\sigma^2}}}{\pi}\frac{dz}{\sigma}\frac{dz'}{\sigma}\right)(y-y')\frac{d\Gamma}{dy}(y')\,dy' \\ &= \frac{1}{U_\infty}\frac{1}{4\pi}\int_{-b/2}^{b/2}\left[\iint_{-\infty}^{\infty}\frac{1}{\pi}\frac{e^{-\frac{z'^2+z^2}{\sigma^2}}}{((y-y')^2+(z-z')^2)}\frac{dz'}{\sigma}\frac{dz}{\sigma}\right](y-y')\frac{d\Gamma}{dy}(y')\,dy',\end{aligned} \tag{37}$$

where we computed the integrals in x, x'. The remaining integrals have to be evaluated numerically.

2. *Application to the elliptical wing and comparison*

Results for the elliptical wing regularized with the 2-D (x-z slice) kernel are presented and compared to those from the 3-D regularization, for a single value of $\sigma/b = 1/32$. For both regularizations, the differences between the two downwash evaluations (mean or centerline evaluation) are also emphasized.

Regarding the circulation distribution, it appears, from Fig. 7, that the 3-D regularization using the mean downwash has the largest difference with the reference case. Even though the formulation is not mathematically justified, the use of the downwash evaluation at the centerline virtually reduces the difference, and especially its maximum value, for the 2-D and 3-D regularizations. As to the circulation obtained with the 2-D regularization, it compares more favorably to the reference case than that obtained with the 3-D smoothing, as expected.

Once again, we relate this behavior to the downwash distribution (Fig. 8). As described above, the 3-D regularization kernel explicitly introduces a smoothing in the spanwise direction. The 2-D regularization conserves a discontinuity in the derivative of the downwash angle at the tip, which is more in line with the reference case. However, in both regularized cases, the downwash angle itself is continuous at the tip, because of the regularization in the vertical direction.

From these results it can be seen that the PLL with downwash evaluation at the centerline always produces results closer to the singular case than the formulation which uses the mean downwash evaluation. This is explained by the fact that using the centerline downwash evaluation virtually removes the regularization from the right hand side of Eq. (23). The resulting problem fortuitously produces a solution closer to that of the singular case. Taking advantage of this property could justify the use of the centerline downwash evaluation if one desires to stay as close as possible to the singular case. However, if one needs to use the present mathematically-consistent formulation, it was shown in Sections III and IV that the regularization must involve the mean downwash angle evaluation.

Transposed to the context of numerical methods, this means that the use of the centerline downwash evaluation will provide results as close as possible to those of the singular PLL (in the sense that they minimize the integral of the squared error on the circulation distribution). We recommend this option in methods where the mollification is necessary for numerical reasons (like in the regular ALM).

However, if the objective is to obtain a consistent mollified method (e.g. if the computational mesh allows for a small σ/c ratio and if the mollification is introduced to support a physical argument rather than as a numerical trick, as in the Advanced Actuator Line [12]), then the the mean downwash evaluation should be used. When it is possible, we discourage the use of an additional spanwise regularization as it introduces a spurious mollification in the circulation and downwash distributions.

C. 1-D (Vertical) Gaussian Regularization

We recall the 1-D Gaussian regularization kernel (Eq. (11)), spanning over the vertical direction only,

$$\xi_\sigma(\mathbf{x}) = \delta(x)\delta(y)\left(\frac{1}{\sqrt{\pi}\,\sigma} e^{-\frac{z^2}{\sigma^2}}\right).$$

This kind of smoothing is actually used in a numerical method proposed in [20–22]. Notice that the latter is not formulated as an ALM, but the line is seen as a vorticity source instead. There is no smoothing in x.

Interestingly, we show that the present case of 1-D vertical regularization yields the exact same integrals as those obtained in the case of the 2-D slice regularization derived above.

The vertical velocity induced at $x = 0$ by the shed vorticity is computed using the Biot-Savart law on the z-mollified vorticity $\boldsymbol{\omega}_{\sigma,s}$,

$$
\begin{aligned}
u_{\sigma,s,z}(y,z) &= \left((\mathbf{K}(\mathbf{x})) * \left(H(x)\ \left(-\frac{d\Gamma}{dy}(y)\right)\ \xi_\sigma(z)\right)\right)\cdot\hat{\mathbf{e}}_z \\
&= \frac{1}{2}\left((\mathbf{K}^{2D}(y,z)) * \left(\left(-\frac{d\Gamma}{dy}(y)\right)\ \xi_\sigma(z)\right)\right)\cdot\hat{\mathbf{e}}_z \\
&= \frac{1}{2}\frac{1}{2\pi}\int_{-b/2}^{b/2}\left(\int_{-\infty}^{\infty}\frac{(y-y')}{((y-y')^2+(z-z')^2)}\,\frac{e^{\frac{-z'^2}{\sigma^2}}}{\sqrt{\pi}}\,\frac{dz'}{\sigma}\right)\left(-\frac{d\Gamma}{dy}(y')\right)dy'.
\end{aligned}
\tag{38}
$$

Evaluating the velocity at the centerline leads to the exact same expression as Eq. (36) for the centerline downwash angle,

$$
\begin{aligned}
\varepsilon_{\sigma,0}(y) &= \frac{1}{U_\infty}\frac{1}{4\pi}\int_{-b/2}^{b/2}\left[\int_{-\infty}^{\infty}\frac{1}{\sqrt{\pi}}\frac{e^{-\frac{z'^2}{\sigma^2}}}{((y-y')^2+z'^2)}\frac{dz'}{\sigma}\right](y-y')\frac{d\Gamma}{dy}(y')\,dy' \\
&= \frac{1}{U_\infty}\frac{1}{4\pi}\int_{-b/2}^{b/2}\left[\sqrt{\pi}\frac{|y-y'|}{\sigma}\,\mathrm{erfc}\left(\frac{|y-y'|}{\sigma}\right)e^{\frac{|y-y'|^2}{\sigma^2}}\right]\frac{1}{(y-y')}\frac{d\Gamma}{dy}(y')\,dy'.
\end{aligned}
\tag{39}
$$

The mean downwash angle is obtained as

$$
\bar{\varepsilon}_\sigma(y) = \frac{1}{U_\infty}\frac{1}{4\pi}\int_{-b/2}^{b/2}\left[\iint_{-\infty}^{\infty}\frac{1}{\pi}\frac{e^{-\frac{z'^2+z^2}{\sigma^2}}}{((y-y')^2+(z-z')^2)}\frac{dz'}{\sigma}\frac{dz}{\sigma}\right](y-y')\frac{d\Gamma}{dy}(y')\,dy', \tag{40}
$$

which is the same expression as Eq. (37). Therefore, the results obtained with the 1-D (z, vertical) regularization are identical to those obtained with the 2-D (x-z slice) regularization.

Again, it was shown that the formulation of the problem is not sensitive to the regularization in the streamwise direction. This has also been observed above in the case of the 3-D regularization compared to the (y-z) only regularization (see Eqs. (29) and (30) vs. Eqs. (33) and (34)). It is also true for the 2-D slice regularization compared to the z only regularization.

IV. Mollified PLL with spanwise variable smoothing

In this section, the smoothing is generalized to the case of regularizations with a variable smoothing length scale in the spanwise direction. As mentioned in the introduction, such regularizations were exploited in [15, 16], using a 3-D Gaussian function, and in [18] using the quasi 2-D regularization function of the ACE. We notice that both used pointwise velocity sampling (equivalent to our definition of $\varepsilon_{\sigma,0}$) instead of a mean value (resp. $\bar{\varepsilon}_\sigma$).

Taking advantage of the present lifting line framework, variable smoothing length scale mollifications can also be studied. We define the mollified vorticity as

$$\begin{aligned}
\tilde{\boldsymbol{\omega}}_\sigma(\mathbf{x}) &= \int_\Omega \xi_{\sigma(\mathbf{x}')}(\mathbf{x}-\mathbf{x}')\, \boldsymbol{\omega}_\delta(\mathbf{x}')\, d\mathbf{x}' \\
&= \underbrace{\int_{-b/2}^{b/2} \xi_{\sigma(y')}(x, y-y', z)\, \Gamma(y')\, dy'}_{\omega_{\sigma,b}}\ \hat{\mathbf{e}}_y \\
&\quad + \underbrace{\int_{-b/2}^{b/2}\int_{-\infty}^{\infty} \xi_{\sigma(y')}(x-x', y-y', z) \left(-H(x')\,\frac{d\Gamma}{dy}(y')\right) dx'\, dy'}_{\omega_{\sigma,s}}\ \hat{\mathbf{e}}_x. \qquad (41)
\end{aligned}$$

As opposed to $\boldsymbol{\omega}_\delta$, this vorticity field is generally not divergence free, and we have $\nabla \cdot \tilde{\boldsymbol{\omega}}_\sigma(\mathbf{x}) = \int_\Omega \nabla\xi_{\sigma(\mathbf{x}')}(\mathbf{x}-\mathbf{x}') \cdot \boldsymbol{\omega}_\delta(\mathbf{x}')\, d\mathbf{x}'$. As explained in [29], a solenoidal vorticity field can be obtained considering an additional term

$$\boldsymbol{\omega}_\sigma(\mathbf{x}) = \int_\Omega \Big(\xi_{\sigma(\mathbf{x}')}(\mathbf{x}-\mathbf{x}')\, \boldsymbol{\omega}_\delta(\mathbf{x}') + \nabla\left(\mathbf{K}_\sigma(\mathbf{x}-\mathbf{x}')\cdot \boldsymbol{\omega}_\delta(\mathbf{x}')\right)\Big) d\mathbf{x}'. \qquad (42)$$

However, as this term is the gradient of a scalar field, it does not contribute to the velocity field. Indeed, recalling that $\nabla^2\mathbf{u}_\sigma = -\nabla \wedge \boldsymbol{\omega}_\sigma$, we obtain that $\nabla^2\mathbf{u}_\sigma = -\nabla \wedge \tilde{\boldsymbol{\omega}}_\sigma$. In other words, when computing the velocity using the Biot-Savart law, we have that

$$\mathbf{u}_\sigma(\mathbf{x}) = U_\infty\, \hat{\mathbf{e}}_x + (\mathbf{K}(\mathbf{x})\wedge) * \boldsymbol{\omega}_\sigma(\mathbf{x}) = U_\infty\, \hat{\mathbf{e}}_x + (\mathbf{K}(\mathbf{x})\wedge) * \tilde{\boldsymbol{\omega}}_\sigma(\mathbf{x}), \qquad (43)$$

and the decomposition proposed in Eq. (14) still holds. Additionally, the force (Eq. (15)) is obtained equivalently as

$$\frac{\mathbf{F}}{\rho} = \int_\Omega \mathbf{u}_\sigma(\mathbf{x}) \wedge \boldsymbol{\omega}_\sigma(\mathbf{x})\, d\mathbf{x} = \int_\Omega \mathbf{u}_\sigma(\mathbf{x}) \wedge \tilde{\boldsymbol{\omega}}_\sigma(\mathbf{x})\, d\mathbf{x}, \qquad (44)$$

given the symmetry properties of the second term in Eq. (42). The subsequent steps of the development in Section III thus remain unchanged, and we therefore obtain the integro-differential equation (23) again, where the downwash now accounts for the variable smoothing length scale.

Only the 3-D Gaussian regularization with variable smoothing parameter in y will be considered in this work. The regularization function is

$$\xi_{\sigma(\mathbf{x}')}(\mathbf{x}) = \delta(x)\, \left(\frac{1}{\pi\, \sigma(y')^2}\, e^{-\frac{(y^2+z^2)}{\sigma(y')^2}}\right), \qquad (45)$$

using the property that the problem is insensitive to the mollification in x. As in [15], we choose a smoothing length scale proportional to the elliptical chord distribution,

$$\sigma(y) = \sigma_0\sqrt{1-\left(\frac{y}{b/2}\right)^2}. \qquad (46)$$

The two expressions for the downwash are

$$\varepsilon_{\sigma,0}(y) = -\frac{1}{U_\infty}\frac{1}{4\pi}\int_{-b/2}^{b/2}\frac{\left(1-e^{-\frac{(y-y')^2}{\sigma(y')^2}}\right)}{(y-y')}\frac{d\Gamma}{dy}(y')dy'$$

and

$$\bar{\varepsilon}_{\sigma}(y) = \frac{1}{U_\infty}\frac{1}{4\pi}\int_{-b/2}^{b/2}\frac{\left(1-e^{-\frac{(y-y')^2}{(\sigma(y)^2+\sigma(y')^2)}}\right)}{(y-y')}\frac{d\Gamma}{dy}(y')dy',$$

Notice that, in an ALM, arbitrary small values of σ cannot be achieved due to numerical constraints*. Previously cited studies proposed the truncation of $\sigma(y)$ to a minimum affordable value near the tips. This case is also considered here.

As depicted in Fig. 9, three distributions of σ are here compared. For the variable σ, the ratio between the smoothing length scale and the local chord is $\sigma(y)/c(y) \simeq 0.25$, which is compatible with the guidelines proposed in [15].

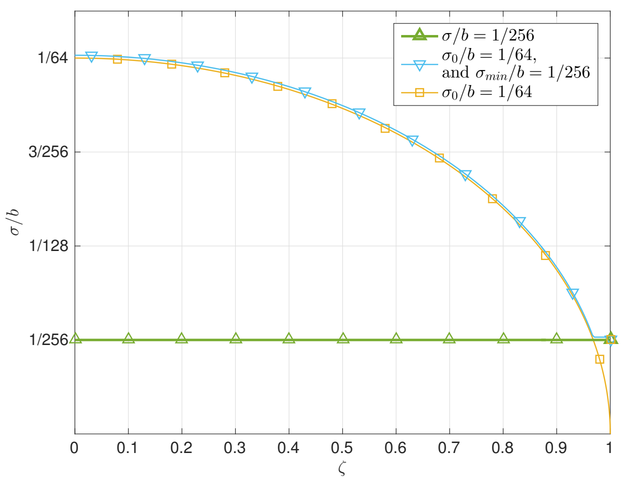

Fig. 9 Distribution of the variable smoothing length scale (with and without truncation) compared to the case of constant σ along the span ($\sigma/b = 1/256$).

Figure 10 shows that the case with variable σ and with downwash evaluation at the centerline has a favorable outlook in terms of circulation distribution. When there is no truncation, the difference with Γ_{ref} monotonically decreases to zero at the tip. Additionally, the evaluation of the downwash angle at the centerline (Fig. 11) yields a constant value across the span, similar to the behavior of the classical PLL. Because σ is zero at $y = \pm\frac{b}{2}$, there is a discontinuity in the downwash velocity at the tip. With truncation, the circulation difference has a maximum close to the tip, just as in the

*In an ALM, forces are applied on the mesh using the regularization kernel. For a given mesh size, there is a minimum value for the volume of that kernel under which the force can't be correctly captured on the grid [15].

constant σ case. As to the downwash angle, a large plateau is observed in the central region, and it finally decreases in the tip region.

A very similar behavior was observed in [16] in the framework of the ALM, and [18] in the ACE. In both references, a fairly constant downwash angle was measured, despite the use of a truncation in σ at the tip. Therefore, our opinion regarding the benefits of a variable σ along the span in numerical methods is that it depends on the available resolution. If the affordable grid size is of the order of the thickness of the blade, then the use of a variable smoothing along the span will likely improve the load distribution relatively to blade resolved CFD, as observed with the Advanced Actuator Line method [12]. Conversely, if the affordable grid size is of the order of (or larger than) the mean chord of the blade, then using a uniform smoothing produces results of the same quality as those using a variable smoothing, provided that the uniform smoothing used (σ_0) is the same as that used for the cutoff value in the variable smoothing ($\sigma_{\min}$).

For the sake of completeness, the lift and drag coefficients are given in Table 2. All cases exhibit similar values.

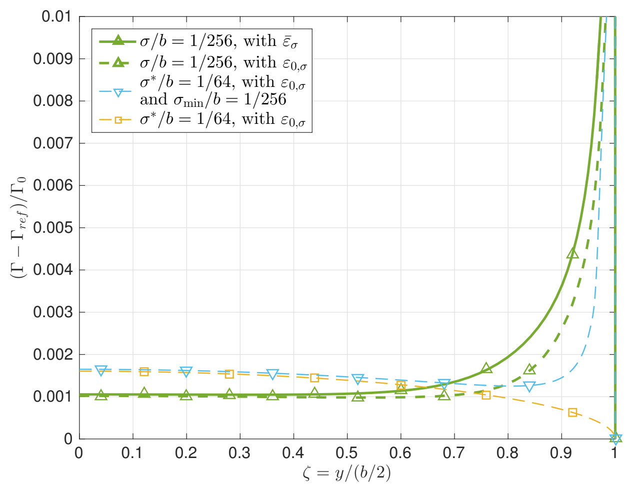

Fig. 10 Difference between the circulation distribution of the mollified PLL and the elliptical distribution, for a 3-D regularization kernel with variable σ and with/without truncation at $\sigma/b = 1/256$.

$\sigma(y)$	σ_0/b	$\sigma_{\min}/b$	eval.	$\frac{C_L}{C_{L,ref}}$	$\frac{C_{D_i}}{C_{D_i,ref}}$
variable	1/32	0	$\varepsilon_{\sigma,0}$	1.002	0.986
variable	1/32	1/256	$\varepsilon_{\sigma,0}$	1.002	0.977
constant	1/256	1/256	$\varepsilon_{\sigma,0}$	1.002	0.982
constant	1/256	1/256	$\bar{\varepsilon}_\sigma$	1.003	0.976

Table 2 Lift and drag coefficients of the mollified PLL for a 3-D regularization kernel, with constant and variable σ and with/without truncation at $\sigma/b = 1/256$.

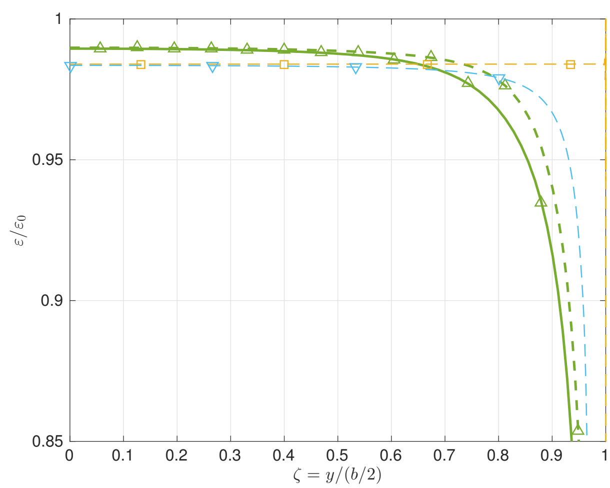

Fig. 11 Downwash angle of the mollified PLL for a 3-D regularization kernel, with variable σ and with/without truncation at $\sigma/b = 1/256$.

V. Conclusions

This work introduced a formalism for the regularization of the classical Prandtl Lifting Line theory. The model for a mollified lifting line was obtained, where the vorticity field introduced by a slender device in the flow field is regularized using an generally anisotropic Gaussian-based smoothing kernel. The integro-differential equation which must be solved to obtain the circulation distribution over the device was derived, and particularized for the 3-D, 2-D and 1-D Gaussian kernels. The equation with a smoothing variable across the span was also obtained.

We showed that the equation to be solved involves the evaluation of a "sectional mean downwash" $\bar{\varepsilon}$ computed using the convolution of the regularized velocity field with the regularization function. Additionally, we obtained that the mollification in the streamwise direction does not modify the final equation. As a result, there is a formal equivalence between the 2-D (slice) and the 1-D (vertical) mollifications considered here.

Lifting lines with various mollifications were then applied to an elliptical wing. As a conclusion of our analyses, the mollification generally induces an increase in the lift coefficient, and a decrease in the induced drag coefficient, relatively to the classical PLL at the same angle of attack. If σ is very small, the reduction in induced drag with respect to the singular case is relatively small, and likely negligible compared to the parasitic drag which would also be present in reality (due to the boundary layers).

It was shown that the results (both in terms of circulation and downwash distributions, and in terms of lift and induced drag coefficients) are quite sensitive to the smoothing kernel used. While the smoothing in the streamwise direction has actually no effect on the results, regularizing in the spanwise direction introduces a filtering operation on the distributions which usually induces large errors in the tip region (compared to the singular case). If possible, it is therefore preferable to remove the smoothing in the spanwise direction, or at least, to use a small smoothing length scale in this direction, in order to obtain results close to the singular case.

In a similar attempt to limit the filtering effect, previous works proposed regularization functions with a variable $\sigma(y)$ defined as a function of the span, and going to some minimum value $\sigma_{\min}$ at the tip. This work showed that the results obtained with such a variable σ approach are actually comparable to those using a smoothing with a uniform $\sigma = \sigma_{\min}$ (at least when it comes to the circulation distribution over an elliptical wing). However, if σ can be taken as small as the local airfoil thickness, other studies showed that the use of a variable smoothing which distributes the forces on a volume corresponding to the shape of the device is likely to improve the load distribution, relatively to blade resolved CFD.

Finally, an alternative formulation of the mollified lifting line consists in replacing the mean downwash $\bar{\varepsilon}_{\sigma}$ by a local evaluation of the downwash $\varepsilon_{\sigma,0}$ at the centerline. Although it is not fully consistent with the framework developed here, results obtained with the latter method showed better agreement with the singular case, even recovering a constant downwash on the elliptical wing.

The presented mollified lifting line provides a simple model which can be advantageously used to compare with and advise on the use of numerical methods such as the Actuator Line Model, Immersed Lifting Lines and other similar methods. In view of our conclusions, we generally recommend the use of the centerline downwash evaluation, in combination with a 2-D or a 1-D regularization, for numerical methods where the smoothing is introduced as a numerical trick. However, in the case of very highly resolved simulations where the smoothing parameter can be chosen almost everywhere regardless of any grid size constraint (except in the tip region), σ can be adapted in order to match the local airfoil thickness. In such conditions, we suggest to opt for a sectional mean downwash evaluation as the resulting approach is more consistent with respect to blade resolved CFD.

Appendix

The induced velocity components can be readily identified from the Biot-Savart law (the kernel of which is $\mathbf{K}(\mathbf{x})\wedge = -(1/||\mathbf{x}^3||)\,\mathbf{x}\wedge$) and the vorticity components. Symmetry properties are also useful when computing the integral of the velocity, the vorticity, or their product, over the whole domain.

	Expression	Symmetries x	Symmetries z
$\omega_{\sigma,b}(\mathbf{x})$	$= +\xi_\sigma(x)\left(\int_{-b/2}^{b/2} \xi_\sigma(y-y')\,\Gamma(y')\,dy'\right)\xi_\sigma(z)$	even	even
$\omega_{\sigma,s}(\mathbf{x})$	$= -H_\sigma(x)\left(\int_{-b/2}^{b/2} \xi_\sigma(y-y')\,\frac{d\Gamma}{dy}(y')\,dy'\right)\xi_\sigma(z)$	–	even
$u_{\sigma,b,x}(\mathbf{x})$	$= [(\mathbf{K}(\mathbf{x})\wedge) * (\omega_{\sigma,b}(\mathbf{x})\hat{\mathbf{e}}_y)]\cdot\hat{\mathbf{e}}_x$	even	odd
	$= +\int_\Omega \frac{(z-z')}{\lvert\lvert(\mathbf{x}-\mathbf{x}')\rvert\rvert^3}\left(\xi_\sigma(x')\left(\int_{-b/2}^{b/2}\xi_\sigma(y'-y'')\,\Gamma(y'')\,dy''\right)\xi_\sigma(z')\right)d\mathbf{x}'$		
	$= [(\mathbf{K}_\sigma(\mathbf{x})\wedge) * (\omega_{\delta,b}(\mathbf{x})\hat{\mathbf{e}}_y)]\cdot\hat{\mathbf{e}}_x$		
	$= +\int_{-b/2}^{b/2}\left[\int_\Omega \xi_\sigma(\mathbf{x}'')\frac{((z-z')-z'')}{\lvert\lvert((\mathbf{x}-\mathbf{x}')-\mathbf{x}'')\rvert\rvert^3}\,d\mathbf{x}''\right]_{x'=z'=0}\Gamma(y')dy'$		
$u_{\sigma,b,z}(\mathbf{x})$	$= [(\mathbf{K}(\mathbf{x})\wedge) * (\omega_{\sigma,b}(\mathbf{x})\hat{\mathbf{e}}_y)]\cdot\hat{\mathbf{e}}_z$	odd	even
	$= -\int_\Omega \frac{(x-x')}{\lvert\lvert(\mathbf{x}-\mathbf{x}')\rvert\rvert^3}\left(\xi_\sigma(x')\left(\int_{-b/2}^{b/2}\xi_\sigma(y'-y'')\,\Gamma(y'')\,dy''\right)\xi_\sigma(z')\right)d\mathbf{x}'$		
	$= [(\mathbf{K}_\sigma(\mathbf{x})\wedge) * (\omega_{\delta,b}(\mathbf{x})\hat{\mathbf{e}}_y)]\cdot\hat{\mathbf{e}}_z$		
	$= -\int_{-b/2}^{b/2}\left[\int_\Omega \xi_\sigma(\mathbf{x}'')\frac{((x-x')-x'')}{\lvert\lvert((\mathbf{x}-\mathbf{x}')-\mathbf{x}'')\rvert\rvert^3}\,d\mathbf{x}''\right]_{x'=z'=0}\Gamma(y')dy'$		
$u_{\sigma,s,y}(\mathbf{x})$	$= [(\mathbf{K}(\mathbf{x})\wedge) * (\omega_{\sigma,s}(\mathbf{x})\hat{\mathbf{e}}_x)]\cdot\hat{\mathbf{e}}_y$	–	odd
	$= -\int_\Omega \frac{(z-z')}{\lvert\lvert(\mathbf{x}-\mathbf{x}')\rvert\rvert^3}\left(H_\sigma(x')\left(\int_{-b/2}^{b/2}\xi_\sigma(y'-y'')\left(-\frac{d\Gamma}{dy}(y'')\right)dy''\right)\xi_\sigma(z')\right)d\mathbf{x}'$		
	$= [(\mathbf{K}_\sigma(\mathbf{x})\wedge) * (\omega_{\delta,s}(\mathbf{x})\hat{\mathbf{e}}_x)]\cdot\hat{\mathbf{e}}_z$		
	$= -\int_{-b/2}^{b/2}\int_0^\infty\left[\int_\Omega \xi_\sigma(\mathbf{x}'')\frac{((z-z')-z'')}{\lvert\lvert((\mathbf{x}-\mathbf{x}')-\mathbf{x}'')\rvert\rvert^3}\,d\mathbf{x}''\right]_{z'=0}\left(-\frac{d\Gamma}{dy}(y')\right)dx'\,dy'$		
$u_{\sigma,s,z}(\mathbf{x})$	$= [(\mathbf{K}(\mathbf{x})\wedge) * (\omega_{\sigma,s}(\mathbf{x})\hat{\mathbf{e}}_x)]\cdot\hat{\mathbf{e}}_y$	–	even
	$= +\int_\Omega \frac{(y-y')}{\lvert\lvert(\mathbf{x}-\mathbf{x}')\rvert\rvert^3}\left(H_\sigma(x')\left(\int_{-b/2}^{b/2}\xi_\sigma(y'-y'')\left(-\frac{d\Gamma}{dy}(y'')\right)dy''\right)\xi_\sigma(z')\right)d\mathbf{x}'$		
	$= [(\mathbf{K}_\sigma(\mathbf{x})\wedge) * (\omega_{\delta,s}(\mathbf{x})\hat{\mathbf{e}}_x)]\cdot\hat{\mathbf{e}}_z$		
	$= +\int_{-b/2}^{b/2}\int_0^\infty\left[\int_\Omega \xi_\sigma(\mathbf{x}'')\frac{((y-y')-y'')}{\lvert\lvert((\mathbf{x}-\mathbf{x}')-\mathbf{x}'')\rvert\rvert^3}\,d\mathbf{x}''\right]_{z'=0}\left(-\frac{d\Gamma}{dy}(y')\right)dx'\,dy'$		

Acknowledgments

Denis-Gabriel Caprace is a Research Fellow of the Fonds de la Recherche Scientifique – FNRS.

References

[1] Prandtl, L., *Tragflügeltheorie*, Göttinger Nachrichten, Mathematisch- Physikalische Klasse, Germany, 1918, pp. 451–477.

[2] Prandtl, L., "Application of Modern Hydrodynamics to Aerodynamics," Technical Report 116, NACA, Jan 1923.

[3] Guermond, J.-L., "A generalized lifting-line theory for curved and swept wings," *Journal of Fluid Mechanics*, Vol. 211, 1990, pp. 497–513.

[4] Phillips, W., and Snyder, D., "Modern adaptation of Prandtl's classic lifting-line theory," *Journal of Aircraft*, Vol. 37, No. 4, 2000, pp. 662–670.

[5] Phlips, P., East, R., and Pratt, N., "An unsteady lifting line theory of flapping wings with application to the forward flight of birds," *Journal of fluid mechanics*, Vol. 112, 1981, pp. 97–125.

[6] Ahmadi, A. R., and Widnall, S. E., "Unsteady lifting-line theory as a singular perturbation problem," *Journal of Fluid Mechanics*, Vol. 153, 1985, pp. 59–81.

[7] Sclavounos, P., "An unsteady lifting-line theory," *Journal of engineering mathematics*, Vol. 21, No. 3, 1987, pp. 201–226.

[8] Glauert, H., *The Elements of Aerofoil and Airscrew Theory*, The University Press, 1926.

[9] McCormick, B. W., *Aerodynamics, aeronautics, and flight mechanics*, John Wiley, 1995.

[10] Rasmussen, M., and Smith, D., "Lifting-line theory for arbitrarily shaped wings," *Journal of Aircraft*, Vol. 36, No. 2, 1999, pp. 340–348.

[11] Sorensen, J. N., and Shen, W. Z., "Numerical modeling of wind turbine wakes," *Journal of Fluids Engineering - Transactions of the ASME*, Vol. 124, No. 2, 2002, pp. 393–399. doi:10.1115/1.1471361.

[12] Churchfield, M. J., Schreck, S., Martinez-Tossas, L. A., Meneveau, C., and Spalart, P. R., "An Advanced Actuator Line Method for Wind Energy Applications and Beyond," *35th Wind Energy Symposium*, 2017, p. 1998.

[13] Benard, P., Viré, A., Moureau, V., Lartigue, G., Beaudet, L., Deglaire, P., and Bricteux, L., "Large-Eddy Simulation of wind turbines wakes including geometrical effects," *Computers & Fluids*, 2018.

[14] Breton, S.-P., Sumner, J., Sørensen, J. N., Hansen, K. S., Sarmast, S., and Ivanell, S., "A survey of modelling methods for high-fidelity wind farm simulations using large eddy simulation," *Phil. Trans. R. Soc. A*, Vol. 375, No. 2091, 2017, p. 20160097.

[15] Jha, P. K., Churchfield, M. J., Moriarty, P. J., and Schmitz, S., "Guidelines for Volume Force Distributions Within Actuator Line Modeling of Wind Turbines on Large-Eddy Simulation-Type Grids," *Journal of Solar Energy Engineering*, Vol. 136, No. 3, 2014, pp. 031003–031003.

[16] Shives, M., and Crawford, C., "Mesh and load distribution requirements for actuator line CFD simulations," *Wind Energy*, Vol. 16, No. 8, 2013, pp. 1183–1196.

[17] Martínez-Tossas, L., Churchfield, M., and Meneveau, C., "Optimal smoothing length scale for actuator line models of wind turbine blades based on Gaussian body force distribution," *Wind Energy*, 2017.

[18] Jha, P. K., and Schmitz, S., "Actuator curve embedding – an advanced actuator line model," *Journal of Fluid Mechanics*, Vol. 834, 2018. doi:10.1017/jfm.2017.793.

[19] Scheurich, F., and Brown, R. E., "Modelling the aerodynamics of vertical-axis wind turbines in unsteady wind conditions," *Wind Energy*, Vol. 16, No. 1, 2013, pp. 91–107. doi:10.1002/we.532.

[20] Chatelain, P., Backaert, S., Winckelmans, G., and Kern, S., "Large Eddy Simulation of wind turbine wakes," *Proceedings of The 9th International Symposium on Engineering Turbulence Modelling and Measurements (ETMM-9), June 6–8, 2012, Thessaloniki, Greece*, Flow, Turbulence and Combustion, Vol. 91, edited by W. Rodi, ERCOFTAC, Springer, 2013, pp. 587–605. doi:10.1007/s10494-013-9474-8.

[21] Chatelain, P., Duponcheel, M., Caprace, D.-G., Marichal, Y., and Winckelmans, G., "Vortex particle-mesh simulations of vertical axis wind turbine flows: from the airfoil performance to the very far wake," *Wind Energy Science*, Vol. 2, No. 1, 2017, p. 317.

[22] Chatelain, P., Duponcheel, M., Zeoli, S., Buffin, S., Caprace, D.-G., Winckelmans, G., and Bricteux, L., "Investigation of the effect of inflow turbulence on vertical axis wind turbine wakes," *Journal of Physics: Conference Series*, Vol. 854, No. 1, 2017, p. 012011.

[23] Kutta, W., "Auftriebskräfte in strömenden Flüssigkeiten," *Illustrierte Aeronautische Mitteilungen*, Vol. 6, No. 133, 1902, pp. 133–135.

[24] Joukowski, N., "Sur les tourbillons adjoints," *Transcript of the Physical Section, Imperial Society of Friends of Natural Sciences, Moscow*, Vol. 23, 1906.

[25] Saffman, P. G., *Vortex dynamics*, Cambridge Monographs on Mechanics, 1995.

[26] Noca, F., "On the evaluation of instantaneous fluid-dynamic forces on a bluff body," Report FM96-5, GALCIT, 1996.

[27] Winckelmans, G. S., "Topics in vortex methods for the computation of three-and two-dimensional incompressible unsteady flows," Ph.D. thesis, California Institute of Technology, 1989.

[28] DLMF, "*NIST Digital Library of Mathematical Functions*," http://dlmf.nist.gov/, Release 1.0.18 of 2018-03-27. URL `http://dlmf.nist.gov/`, f. W. J. Olver, A. B. Olde Daalhuis, D. W. Lozier, B. I. Schneider, R. F. Boisvert, C. W. Clark, B. R. Miller and B. V. Saunders, eds.

[29] Winckelmans, G. S., and Leonard, A., "Contributions to Vortex Particle Methods for the Computation of Three-Dimensional Incompressible Unsteady Flows;," *Journal of Computational Physics*, Vol. 109, No. 2, 1993, pp. 247–273.